Acta Materialia 196 (2020) 44–51

Contents lists available at ScienceDirect

Acta Materialia

journal homepage: www.elsevier.com/locate/actamat

Full length article

Segregation of Ni at early stages of radiation damage in NiCoFeCr solid solution alloys

F. Tuomisto[a,b,c,*], I. Makkonen[a,b,c], J. Heikinheimo[a], F. Granberg[c], F. Djurabekova[b,c], K. Nordlund[c], G. Velisa[d,1], H. Bei[d], H. Xue[e], W.J. Weber[d,e], Y. Zhang[d,e]

[a] Department of Applied Physics, Aalto University, POB 15100, 00076, Aalto, Finland
[b] Helsinki Institute of Physics, University of Helsinki, POB 43, 00014, Helsinki, Finland
[c] Department of Physics, University of Helsinki, POB 43, 00014, Helsinki, Finland
[d] Materials Science and Technology Division, Oak Ridge National Laboratory, Oak Ridge, TN, 37831, USA
[e] Department of Materials Science and Engineering, The University of Tennessee, Knoxville, TN, 37996, USA

ARTICLE INFO

Article history:
Received 27 February 2020
Revised 13 May 2020
Accepted 13 June 2020
Available online 18 June 2020

ABSTRACT

Defect evolution under irradiation is investigated in a set of single-phase concentrated solid solution alloys (SP-CSAs) containing Ni with Co, Fe and/or Cr. We show that atomic segregation of Ni takes place already at very early stages of radiation damage in the 2–4 element SP-CSAs containing Fe or Cr, well below 1 dpa. We arrive at this conclusion by following the evolution of positron annihilation signals as a function of irradiation dose in single crystal samples, complemented by molecular dynamics simulations in the same model systems for high entropy alloys (HEAs). This manifestation of short-range order calls attention to composition fluctuations at the atomic level in irradiated HEAs. Ion irradiation may induce short-range order in certain alloys due to chemically biased elemental diffusion. The work highlights the necessity of updating the assumption of a totally random arrangement in the irradiated alloys, even though the alloys before irradiation have random arrangements of different chemical elements.

1. Introduction

Endeavors of improving the performance of structural materials for nuclear energy applications have been a constant effort for many decades, including improvements in mechanical properties, corrosion resistance and radiation tolerance. Increasing demands for energy and the requirement of safe operations of power plants that produce it have raised the need for innovative material discoveries of structural alloys that can withstand extreme reactor environments of high temperature and harmful radiation flux. New, non-intrusive, non-traditional metallic alloys that would meet all requirements of structural materials over desired life times are highly wanted.

The development of metallic alloys is arguably one of the everlasting advances of humankind. In the long history of alloy development, solid solution strengthening is one of the most widely used methods to achieve specific desirable properties. Most research and applications have been focused on alloys with one or two principal elemental species, to which the addition of alloying elements at low concentrations has been used to give various performance enhancements. Such traditional approaches by taking a material with empirically good properties and making small changes in composition and microstructure to achieve a more desired performance, do not fully meet the challenges imposed by the extreme environments. In sharp contrast to traditional dilute alloys, recent success in the synthesis of multicomponent single-phase concentrated solid solution alloys (SP-CSAs), including high entropy alloys (HEAs) that commonly contain four or more alloying elements, has opened new frontiers in materials research [1–10]. As opposed to traditional alloys that populate the corners of phase diagrams, SP-CSAs (and HEAs) occupy the center of the diagrams that vastly expands the compositional space available for alloy discovery. In these CSAs, a random arrangement of multiple elemental species on a regular lattice, such as face-centered cubic (fcc) or body-centered cubic (bcc), results in unique site-to-site lattice distortions and local disordered chemical environments

* Corresponding author at: Department of Physics, University of Helsinki, POB 43, 00014, Helsinki, Finland.
E-mail address: filip.tuomisto@helsinki.fi (F. Tuomisto).
[1] Current address: Horia Hulubei National Institute for Physics and Nuclear Engineering, P.O.B. MG-6, 077125 Magurele, Romania.

https://doi.org/10.1016/j.actamat.2020.06.024

[6–11]. Research has rapidly shown that compositional variations in SP-CSAs have an enormous impact on defect dynamics and generate impressive properties, including exceptional fracture toughness at cryogenic temperatures, high strength and low plasticity at elevated temperatures [1–5], enhanced radiation tolerance [6,8–10], and improved corrosion resistance [11–14].

Displacement damage from fast neutrons, fission fragments, and associated energetic recoils cause displacements of atoms from their lattice sites, thereby forming atomic-scale defects. The knowledge of radiation damage in traditional dilute metal alloys is described well by various experimental and computational studies [15–20] that allow improvement of the understanding and controllability of material properties. Recently, irradiation studies in SP-CSAs have shown that varying the type and concentration of alloying elements alter the local electronic and atomic environments [6,8,9], which can significantly influence defect energetics [21]. By tuning the composition of SP-CSAs, radiation damage tolerance is improved [6–9]. Under high-temperature and high-dose irradiations, some binary, ternary and quaternary SP-CSAs, as well as NiCoFeCrMn HEA, have shown ~ 20 to 30 times lower volume swelling than that of Ni [6,7,9]. In traditional dilute alloys, the trapping of point defects by solute atoms has a significant influence on the radiation-induced segregation (RIS), resulting from preferential interaction between the flux of vacancies/interstitials and the flux of solutes to point defect sinks [17–19]. In solid solution CSAs, RIS has also been reported and significant gradients in local chemistry may exist [22,23]. In recent work [22], NiCoFeCrMn and NiCoFeCrPd HEAs were irradiated with 1250 kV electron irradiations, the condition in which only Frenkel pairs are expected to be produced, at 400 °C up to 1 displacement per atom (dpa). The results suggested that Cr/Fe/Mn/Pd deplete and Co/Ni accumulate at radiation-induced dislocation loops. The authors concluded that the actively segregating elements are alloy-specific and primarily determined by elemental difference – for example, Pd is much larger and heavier than the other alloying elements. Under ion irradiation where both point defects and small defect clusters are formed as the primary damage state [23,24], the authors however observe no obvious RIS near the loops in NiCoFeCrMn, and conclude that RIS is significantly reduced with increasing compositional complexity. A possible explanation is offered by another recent work [25], which indicates that under ion irradiation conditions, the heat spikes can lead to interatomic mixing that counteracts elemental segregation. At the present time, contrary to traditional alloys with low solute concentration in single or multiple phases, the underlying mechanisms contributing toward enhanced irradiation resistance and outstanding mechanical performance of these non-traditional CSAs are still unclear, and especially little is known on the early stage of production and evolution of vacancy-type defects. As microstructures in SP-CSAs evolve under irradiation, the accompanying elemental segregation is unknown, and the associated material performance of SP-CSAs with extreme compositional disorder is an unexplored frontier in materials science.

Atomic-level transport properties, for example chemically-biased point defect diffusion [26,27] or 1-D gliding self-interstitial atoms clusters [28], are at the core of material performance under extreme conditions, either separate or combined, such as large load bearing, high pressure, shockwaves and radiation that drive materials out of equilibrium phases. Most of today's knowledge of electronic or inelastic energy dissipation and the early stages of radiation damage is based on theoretical modeling and computer simulations of these non-equilibrium to equilibrium transitions. Information on what is created after the initial stage of ion-solid interaction – after atoms are displaced due to kinetic/elastic energy transfer and local electronic excitation, resulting in defect production and damage evolution right following the initial energy deposition – is largely unknown. Recent studies have shown that modification of compositional complexity alters the defect dynamics at the early stage of radiation damage, demonstrated by the remarkable suppression of damage accumulation [6,29], as well as the microstructural changes at the later stage, demonstrated by a substantial reduction in void swelling [7,9]. Hence knowledge on the early stages of radiation damage, when defects are created following the transfer, equilibration, and dissipation of simultaneous elastic and inelastic energy deposition, is critical to reveal a material's ability to dissipate radiation energy and to predict the material's response to particle irradiation.

In this work, we show that elemental segregation takes place already at very early stages of radiation damage in SP-CSAs, well below 1 dpa. The six most commonly studied fcc single crystals of elemental nickel, binaries NiCo and NiFe, ternaries NiCoCr and NiCoFe, and quaternary NiCoFeCr, all at equiatomic ratios, are chosen for investigation. These model crystals are composed solely of 3*d* transition metals, i.e., limited difference in atomic mass and size but with increasing differences in the 3*d* electron count [30], and therefore expected to reveal unique defect properties resulting from distinct electronic structures and atomic arrangements. By performing positron annihilation experiments on as-grown (non-irradiated) and irradiated crystals, associated electronic structure calculations, and molecular dynamics simulations, we show that atomic-level segregation of Ni around mono-vacancy-type damage takes place in the Fe and Cr containing alloys. Interestingly, this segregation appears to be correlated with improved radiation resistance, suggesting an intriguing coupling between the short-range order and mechanical properties in these alloys.

2. Methods

2.1. Positron annihilation spectroscopy

Positron annihilation spectroscopy is a collection of effective methods for the investigation of vacancy-type point defects in crystalline solids [31]. Positron lifetime was measured in unirradiated samples with a digital coincidence spectrometer with a time resolution of 250 ps. Two sample pieces were sandwiched with a 1 MBq positron source (^{22}Na deposited on 1.5 μm Al foil). Typically 2×10^6 annihilation events are collected in each positron lifetime spectrum. The lifetime spectrum $n(t) = \Sigma_i I_i \exp(-t/\tau_i)$ was analyzed as the sum of exponential decay components convoluted with the Gaussian resolution function of the spectrometer, after subtracting the constant background and annihilations in the source material (typically a few percent, for details see, *e.g.*, [31]). Doppler broadening measurements of positron annihilation radiation were performed in the irradiated samples with a variable-energy positron beam. Positron implantation energies were varied from 0 to 25 keV, corresponding to mean implantation depths up to 0.8 μm (information depth 1.6 μm). We used high purity germanium (HPGe) detectors with an energy resolution of 1.2 keV at 511 keV. The integration windows for the S and W parameters were set to $|p_L| < 0.4$ a.u. and 1.6 a.u. $< |p_L| < 4.0$ a.u., respectively. In addition to the S and W parameters, effective positron diffusion lengths were extracted from the depth-resolved data through fitting the stationary positron diffusion equation [32].

We used ab initio electronic structure calculations to model the positron annihilation parameters in the metal lattices (Ni, Co, Cr and Fe) and at different kinds of vacancy defects, taking into account the forces exerted on the ions by the localized positron [33,34]. The valence electron densities were obtained self-consistently via the local-density approximation (LDA), employing the projector augmented-wave (PAW) method [35] and the plane-wave code VASP [36–38]. The positron states and annihilation characteristics were determined using the LDA [39] and the state-dependent scheme [40] for the momentum densities of an-

nihilating electron-positron pairs. We use a 32-atom fcc supercell. The Doppler spectra and the S and W parameters were computed using reconstructed PAW orbitals and atomic orbitals [33,34] for the core electrons, and finally convoluted with the experimental resolution function. Results for the alloys were constructed by averaging of the elemental data.

2.2. Crystal growth

Pure Ni crystal and single-phase NiCo, NiFe, NiCoCr, NiCoFe, NiCoFeCr equiatomic solid solution alloys were prepared using high-purity Ni, Co, Fe and Cr elemental metals (> 99.9%) by arc melting, drop casting, solidification, and crystallization [8,9]. Before drop-casting into cylindrical copper molds, the mix was flipped, re-melted and re-mixing five times to ensure a homogeneity. The polycrystalline drop-cast ingots were then loaded into an optical floating zone furnace and converted to a single crystal. The crystals were oriented and cut ~1 mm thickness normal to the [100] directions by electro-discharge machining, the surfaces were electrochemically polished to remove surface damage from the cutting process and to produce damage-free surfaces for ion irradiations. These (100)-oriented single fcc phase crystals are high-quality crystals with random arrangements of the chemical elements and few crystal imperfections [41]. The quality [6–8,29] and the randomness [11,42,43] have been studied and confirmed experimentally by ion channeling methods, transmission electron microscopy techniques, X-ray or neutron total scattering and extended X-ray absorption fine structure (EXAFS), X-ray diffraction and X-ray scattering techniques.

2.3. Ion irradiation

The Ni ion irradiations were performed at the Ion Beam Materials Laboratory (IBML) at the University of Tennessee in partnership with Oak Ridge National Laboratory [41]. The MeV Ni ion irradiations produce a recoil spectrum similar to fast neutrons and do not cause transmutations that could lead to high radioactivity of the samples [44]. In addition, ion beams produce energetic recoils that lead to very localized (i.e., a few nanometers) but extremely high pressures and temperatures [45]. Such energetic ions can be applied as a unique tool to study materials response under extreme conditions and to modify materials for desirable properties. The irradiations were performed at room temperature in order to minimize the possible modification of previous irradiated regions and 5° off the surface normal to avoid channeling implantation. In order to produce wide and more uniform damage to a depth beyond 3.0 μm for positron experiments, samples were irradiated using Ni ions with multiple energies (2, 4, 8 and 16 MeV). The irradiation sequence was from higher energies to lower energies in order to minimize modification of pre-existing defects created by earlier irradiations. The depth profile of irradiation-induced in displacements per atom (dpa) was calculated using the Stopping and Range of Ions in Matter (SRIM) code [46] using the full cascade option [47]. The measured sample densities of 8.908, 8.848, 8.232, 8.273, 8.390 and 8.144 g cm^{-3} for Ni, NiCo, NiFe, NiCoCr, NiCoFe, and NiCoFeCr, respectively, were used, along with an assumed threshold displacement energy of 40 eV for all elements [48]. The essential ion fluences for each ion energy were then chosen based on the SRIM calculations to produce doses range from 0.01 dpa to 1 dpa. An example of 1 dpa profile is shown in Fig. 1 resulting from multiple energies Ni ion irradiations in NiCoFeCr. Table 1 shows the fluences for each irradiation condition. Note that the average dpa values in the table refer to the whole irradiated range, while at the depth scale probed by positrons the average dpa is slightly lower (e.g., roughly 0.8 dpa for the 0.9 dpa irradiation). Nevertheless, we refer to the samples by rounded dose values in an order-of-magnitude fashion, given in parentheses in the table. The average concentration of implanted Ni in the damaged region is roughly 3 × 10^{18} cm^{-3} / dpa. For all the irradiations, the Ni ion flux was kept at 4.5 × 10^{10} ion cm^{-2} s^{-1}.

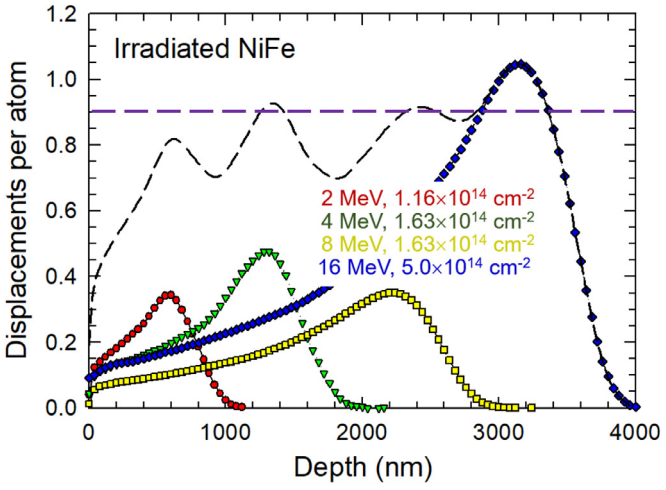

Fig. 1. SRIM-predicted dpa profile for the NiFe sample, assuming the density of 8.232 g cm^{-3}, irradiated with multiple energies of Ni ions. The Ni energies and the corresponding fluences are indicated on the plot. The purple dashed line represents the average dpa level for this irradiation sequence, corresponding to an average Ni concentration of 3 × 10^{18} cm^{-3}.

2.4. Molecular dynamics simulations and analysis

To obtain a picture of radiation damage at elevated doses, massively overlapping 5 keV cascades were simulated at room temperature in molecular dynamics (MD) [49,50]. This choice of cascade energy yields the desired doses with reasonably sized simulation cells, while it still is high enough to be in the heat spike regime [51]. The materials investigated were the same as the ones in the experimental setup, with the exclusion of NiCoFeCr. The details of these simulations are briefly described in the supplementary material and more thoroughly in [50]. These kinds of simulations have been validated for CSAs against experiments, with very good agreement [52]. The Ni ion energies in the employed range (see Table 1) are such that the primary knock-on atom (PKA) spectra do not change dramatically and hence the same approach can be used for all ion energies [53]. The simulation cells were analyzed at different doses, to study the vacancy concentrations and vacancy cluster statistics. To reduce statistical fluctuations, the results at each dose are the value at the exact dose plus and minus three cascades, so in total seven frames per run and material. The space filling Wigner-Seitz cell method was utilized to observe the vacancies. A cutoff in the middle between the second nearest neighbor and the third nearest neighbor was used to consider vacancies to belong to the same cluster. In addition to the number of vacancies and vacancy cluster statistics, the detailed neighborhood of the vacancies and vacancy clusters were analyzed in form of elemental segregation to these defects. In this analysis, the nearest neighbor atoms of the vacancies were analyzed through a cutoff in the middle between the first and second nearest neighbor. For the vacancy cluster, the neighborhood of each and every vacancy building up the cluster was analyzed and the statistics of all the cluster vacancies was combined to get the elemental statistics of the clusters.

3. Results

Ni ion irradiations with 4 different energies and ion fluences were performed in the model crystals to produce a wide dam-

Table 1
Irradiation conditions including the corresponding ion fluences and average damage level in displacements per atom (dpa) estimated from full cascade SRIM simulations [47].

	0.009 dpa (0.01 dpa)	0.027 dpa (0.3 dpa)	0.09 dpa (0.1 dpa)	0.27 dpa (0.3 dpa)	0.9 dpa (1 dpa)
2 MeV	1.16×10^{12} cm^{-2}	3.5×10^{12} cm^{-2}	1.16×10^{13} cm^{-2}	3.5×10^{13} cm^{-2}	1.16×10^{14} cm^{-2}
4 MeV	1.63×10^{12} cm^{-2}	4.9×10^{12} cm^{-2}	1.63×10^{13} cm^{-2}	4.9×10^{13} cm^{-2}	1.63×10^{14} cm^{-2}
8 MeV	1.63×10^{12} cm^{-2}	4.9×10^{12} cm^{-2}	1.63×10^{13} cm^{-2}	4.9×10^{13} cm^{-2}	1.63×10^{14} cm^{-2}
16 MeV	5.0×10^{12} cm^{-2}	1.5×10^{13} cm^{-2}	5.0×10^{13} cm^{-2}	1.5×10^{14} cm^{-2}	5.0×10^{14} cm^{-2}

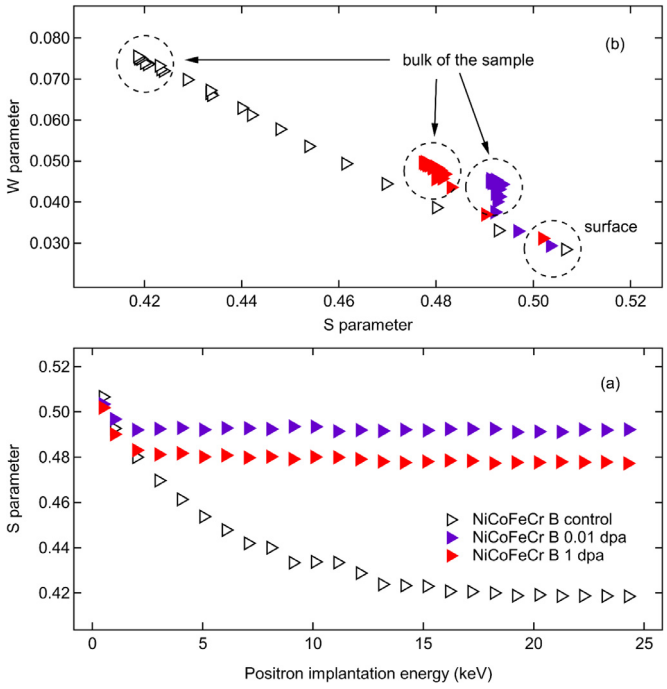

Fig. 2. (a) S parameter measured as a function of the positron implantation energy in selected samples. (b) (S, W) parameters for the same samples, the positron implantation energy is the running parameter in the data points. The error bars are at most the size of the markers.

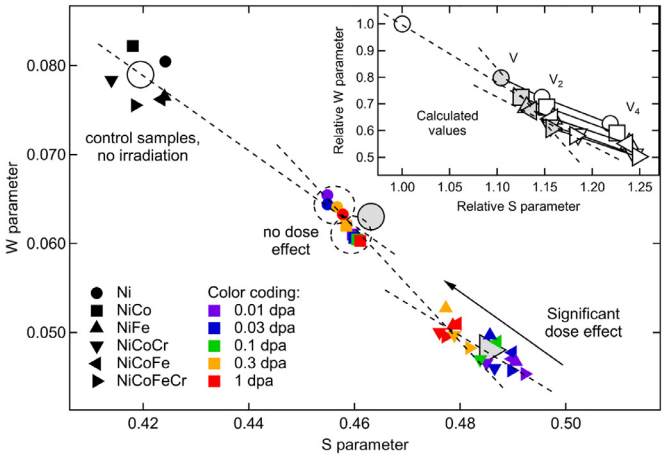

Fig. 3. (S, W) parameters of the irradiated samples, the large empty circle represents the center-of-mass of the control samples. The inset shows theoretical predictions for different sizes of vacancies in the NiCoFeCr systems. The dashed lines in the figure and the inset represent the same slopes. The error bars are at most the size of the markers.

age region close to the surface and to a depth close to 3.5 μm (Fig. 1). Five different damage levels (0.01, 0.03, 0.1, 0.3 dpa and 1 dpa) and totally 45 samples were investigated. Fig. 2a presents the S parameter measured as a function of positron implantation energy in three NiCoFeCr samples: an unirradiated control sample and two irradiated samples with 2 – 16 MeV Ni ions to average doses of 0.01 dpa and 1 dpa. When positrons are implanted close to the sample surface with E $\leq$ 1 keV, corresponding to a penetration depth of up to 10 nm, the same S parameter of S = 0.50-0.51 is recorded in all three samples. The region of the roughly constant S parameter begins above 15 keV implantation energy (corresponding to a mean implantation depth of about 400 nm) in the control sample, and already at about 2 keV in the irradiated samples. The data obtained at these energies are taken as characteristic of the sample. The increased S parameter in the irradiated samples compared to the control sample indicates that the positron-electron momentum distribution is narrower in these samples, a clear sign of vacancy defects created in the irradiated region. The faster transition of the S parameter from the surface values to the values in the bulk of the material in the irradiated samples is a consequence of the effective positron diffusion length shortening with the increase of the density of vacancy defects that trap positrons.

The (S, E) and (W, E) data measured in all the 45 samples are shown in the supplementary material. It is clearly seen that the S parameter increases (W parameter decreases) dramatically with irradiation compared to the un-irradiated control samples. At the same time, it is clearly seen that the effective positron diffusion length shortens significantly as a consequence of the irradiation. Both observations indicate that the control samples provide positron annihilation signals close to those representing the defect-free crystal lattice of each of the alloys. Indeed, fitting the stationary positron diffusion equation [32] simultaneously to the S vs. E and W vs. E data gives values in the range 50–150 nm for the control samples and values in the range 10–50 nm for the irradiated samples. Further, the average positron lifetimes measured in the control samples vary in the range τ_{ave} = 120–135 ps, with the lowest values in the range τ_{ave} = 120–125 ps (single-component spectra) for each of the as-grown alloys. The lattice lifetime, i.e., the lifetime corresponding to the delocalized positron state in the defect-free crystal lattice is roughly τ_B = 110 ps for the elemental metals Ni, Fe, Cr and Co while mono-vacancy lifetimes are in the range 170–180 ps [54–57]. Hence, it is likely that the control samples contain varying albeit small concentrations of dislocation and vacancy-type defects [58], but they are good enough to be used as a point of comparison. The fitted positron diffusion lengths and measured positron lifetimes are shown for all the samples in the supplementary material.

The evolution of the positron annihilation parameters with irradiation is best monitored by investigating the (S, W) plot shown in Fig. 2b. Data points characteristic to different annihilation states are clearly distinguishable as pointed out in the figure. It is clearly seen that the (S, W) points converge to values in the bulk of the samples at high implantation energies. Fig. 3 shows the (S, W) points determined for all the irradiated samples (colored markers) and for the control samples identified as best reference points (black markers), i.e., producing the lowest S, the highest W, the longest effective positron diffusion length and the shortest positron

lifetime. The data points for the control samples are all rather close to each other as expected, as the elemental Ni, Co, Fe and Cr all produce very similar positron data. A random alloy of any of the combinations retaining the lattice structure should produce positron data that is close to a linear combination of the constituents [59].

The main observation in Fig. 3 for the irradiated samples is that for Ni and NiCo the data do not depend on the amount of damage produced in the whole range of the experiments, that is 0.01 – 1 dpa. All the (S, W) points are clustered within the small dashed circles shown in the figure, indicating that the effects of the irradiation on the positron annihilation data are saturated already at the lowest dose. In contrast, the (S, W) points for NiFe, NiCoCr, NiCoFe and NiCoFeCr show a remarkable evolution towards the upper left-hand corner. This phenomenon has escaped observation in earlier experiments in a single alloy with a single irradiation dose [60].

In earlier work, the Doppler broadening parameter for mono-vacancies relative to the parameters in the lattice in elemental Ni have been identified as S_D / S_B = 1.08 – 1.10 [61], corresponding to S = 0.455 – 0.465 in Fig. 3. This indicates that the defects detected in our experiments in irradiated Ni are mono-vacancies, and with high probability this is the case for NiCo as well, where no evolution of the data is observed. For further analysis of this issue, we performed ab initio electronic structure calculations of positron annihilation signals for different sizes of vacancy defects (V, V_2 and V_4) in elemental Ni, Co, Fe and Cr and produced the data for the alloys through linear combination [62]. The calculated Doppler broadening spectra are consistent with measurements performed in elemental metals [63]. The relative S and W parameters for the vacancy defects (vacancy-specific parameters normalized by those of the perfect crystal lattice) are shown in the inset of Fig. 3. As expected, the calculated data show a clear tendency of the (S, W) parameters shifting towards the lower right-hand corner of the figure with increasing vacancy size, as well as a shift (with a different slope) of the (S, W) data with changing alloy composition (the larger the difference in 3*d* electron count, the larger the effect of the mono-vacancy). Two calculated data points are reproduced also among the experimental points using (S, W) = (0.42, 0.079) as an indicative lattice-representing point, showing that the average size of the radiation damage in the experimental data corresponds to mono-vacancies also for the ternary and quaternary alloys. Positrons detecting primarily mono-vacancy-sized defects is in line with the formation of vacancy clusters through mono-vacancy migration not being an efficient process at room temperature, as the mono-vacancy migration barriers are higher than 1 eV in Ni and Ni-based alloys [21].

We have not normalized the experimental (S, W) parameters due to the lack of a well-defined reference point that could be used for normalization. There is some natural scatter in the control samples in Fig. 3 as different alloys are studied, and in addition the lifetime results suggest that the control samples are not completely defect-free (see also the discussion in the supplementary material). Instead, we have used the center-of-mass (S, W) point of the control samples to transfer two calculated points from the inset into the main Fig. 3, in order to compare the theoretical and experimental data in the most illustrative manner. Note that the correlation effects related to positron annihilation with 3*d* shells of the transition metal elements are difficult to describe and parametrize when modeling positron lifetime and Doppler broadening. The LDA enhancement factor overestimates the contribution of these shells, which leads to an overestimated intensity at high momenta. However, for normalized Doppler broadening spectra as well as for normalized S and W parameters (e.g. S/S_B) the systematic discrepancies between experiment and theory have been found to cancel. This is well visible in comparisons made for elemental metals using the same numerical approach and approximations [33,34].

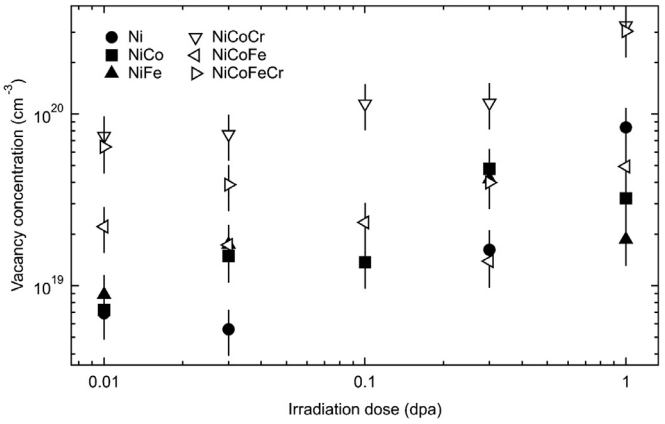

Fig. 4. Vacancy concentrations estimated from positron data. The error bars represent the relative error of concentrations within each alloy.

4. Discussion

The observed evolution of the data points with irradiation dose in NiFe, NiCoCr, NiCoFe and NiCoFeCr can occur for one of the three following reasons: (*i*) reduction in overall vacancy concentration in the irradiated SP-CSAs, (*ii*) change in average vacancy size, or (*iii*) change in the average chemical environment of the detected vacancy defects. We rule out reason (*i*), as the overall vacancy concentration c_D can be estimated from the effective positron diffusion length $L_{\text{eff}}{}^{+}$ through the relation $L^{+}_{\text{eff}} = L^{+}\sqrt{(\tau_B^{-1})/(\tau_B^{-1} + \mu_V c_D)}$, assuming a common positron trapping coefficient of $\mu_V = 10^{15}$ s^{-1} for the vacancy defects [64], diffusion length L^{+} = 160 nm [65], and a common lattice lifetime of τ_B = 110 ps for all the samples. The absolute scale of the vacancy concentrations estimated in this way is correct within an order of magnitude, with the values given here being at the lower end of the range due to the choice of the positron trapping coefficient [64]. The relative error is much smaller, of the order of 25–30% within one alloy, with the uncertainty originating mainly from the assessment of the effective positron diffusion length. Fig. 4 shows the estimated vacancy concentrations for all the samples and shows a clear increase with irradiation dose. The experimentally extracted vacancy concentrations are 1-2 orders of magnitude lower than the predictions from Stopping and Range of Ions in Matter (SRIM) calculations, which can be expected due to the uncertainty in the absolute concentration scale and defect recombination during and after irradiation at room temperature [66]. The estimated vacancy concentrations appear higher in Cr-containing alloys, which may be due to the choice of a common positron diffusion length for all the alloys (see supplementary material for a more detailed discussion). Importantly, the experimental data in Fig. 4 show that the vacancy concentrations increase with increasing irradiation dose in our samples, ruling out explanation (*i*). This is as expected, since a decrease in vacancy concentration with increasing irradiation dose would be unusual.

If the evolution of the (S, W) data with increasing irradiation dose in NiFe, NiCoCr, NiCoFe and NiCoFeCr was due to a change in average vacancy size, this would need to be a reduction as the Doppler broadening of the annihilation spectrum narrows and S parameter increases with increasing open volume [64]. The state-of-the-art theoretical calculations (inset of Fig. 3) show this to be the case for all the alloys. However, a reduction of average vacancy size with increasing irradiation dose, in addition to being counter-intuitive, is opposite to what is predicted by cascade simulations employing molecular dynamics (MD) as shown in Fig. 5. The MD simulations predict that the fraction of mono-vacancies slightly de-

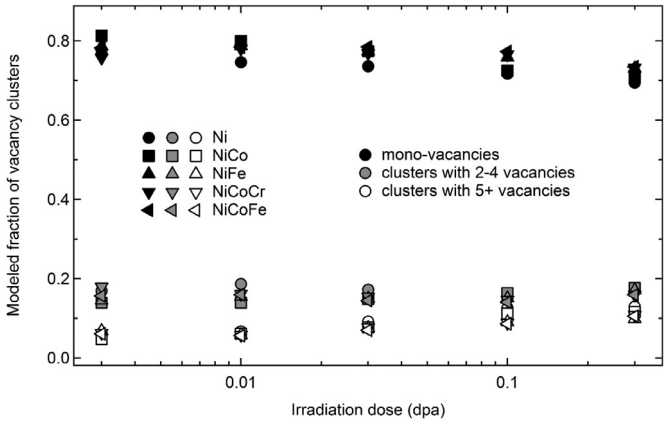

Fig. 5. Modeled fractions of clusters containing different amounts of vacancy defects as a function of irradiation dose. The error bars are at most the size of the markers.

creases and the fraction of larger vacancy clusters slightly increases for all the considered alloys when the irradiation dose is increased. It should be noted that the simulation is also quantitatively in line with the experimental observation that the dominant vacancy type defects in the irradiated materials are of mono-vacancy size at least up to a dose of 0.3 dpa. In addition, the effect of the slight increase in the average vacancy cluster size predicted by the MD simulations can be translated to an increase (decrease) in relative S (W) parameter by 0.01, matching very closely the span and increasing (decreasing) trend of the experimental S (W) parameters in Ni and NiCo as a function of irradiation dose (Fig. 3). On longer timescales, eventual migration of the irradiation-induced vacancy-type defects will further increase the average size of vacancy-type defects in the material. We thus rule out also reason (*ii*), as the experimental data cannot be explained by a change in the average vacancy size with increasing irradiation dose.

Hence, the only possible explanation for the observed evolution of the data is reason (*iii*): we evidence a change in the average chemical environment of the detected vacancy defects with increasing irradiation dose in NiFe, NiCoCr, NiCoFe and NiCoFeCr. The evolution of the (S, W) data towards the data in Ni and NiCo indicates that the average number of Ni and/or Co atoms increases in the 12 atoms surrounding the mono-vacancy in the fcc structure compared to the lowest irradiation doses. This means that the vacancy defects in these higher-dose irradiated alloys have more Ni or Co as nearest neighbors than they would if the distribution of the elements was random. This phenomenon, manifested by the spread of the data points in Fig. 3, appears to get stronger with increasing alloy complexity. The MD simulations show a relative increase of Ni near mono- and di-vacancies in all of the alloys, with the smallest effect in NiCo (51% / 49%) and NiFe (52% / 48%) and slightly larger in NiCoFe and NiCoCr (36% / 33% / 31%). For example, in the NiCoCr alloy this translates to an average of 4.3 Ni atoms, 4.0 Co atoms and 3.7 Cr atoms neighboring the mono-vacancy, as opposed to the alloy average of 4 Ni, 4 Co and 4 Cr atoms. This result is in favor of only Ni segregating, hence allowing us to conclude that we observe directional mass transport of Ni in the multi-component alloys. Interestingly, minor segregation in these kinds of simulations has been earlier correlated with a more drastic segregation on experimental timescales [25,26], where it was observed that radiation mixing and thermodynamics are competing. In recent work on chemically-biased diffusion and segregation in irradiated Ni-Fe SP-CSAs, the integrated results from both experiments and MD simulations show that all sinks (voids, dislocation) are enriched by Ni atoms, supporting our conclusion. The possible underestimation of segregation [25] is due to the very high dose-rates in the simulations compared to experiments, leading to much less time for diffusion and migration. It is important to note the scale at which our observation is valid: the elemental segregation observed by positrons only describes shortest-possible-range ordering phenomena, that is, individual Ni atoms collected next to mono-vacancy defects whose concentrations are in the 100-1000 ppm range.

Interestingly, the strengthening of directional mass transport of Ni is correlated with the radiation resistance that is observed to improve when the number of alloying elements is increased [23]. Recent radiotracer diffusion experiments [67–69] have shown that the diffusivity of the different elements in these alloys is of highly complex nature and depends strongly not only on the matrix but also on the diffusing element. We note that in our room-temperature irradiation experiments we expect the vacancy-type defects to be stable after the ion irradiation induced complex nonequilibrium processes cool down, while interstitials are expected to be still highly mobile [70,71]. Our observation of vacancy-related Ni-preferential elemental segregation on the atomic scale can shed light on the unusual diffusion properties in SP-CSAs. In particular, the different behavior of Ni and NiCo compared to NiFe, NiCoCr, NiCoFe and NiCoFeCr may be attributed to significantly increased sluggish diffusion in the more chemically disordered alloys [27,28,30,72]. This sluggish diffusion is also a possible reason for the trend-like increase in the irradiation-induced vacancy concentrations with increasing alloy complexity, seen in Fig. 4. Interestingly, phenomena related to chemical ordering were not observed in recent work where 0.001 – 1 dpa irradiation damage was produced by 150-keV hydrogen ions [73], suggesting that the spectrum of transferred energy has a significant effect on the ordering.

In disordered CSAs, it is commonly assumed that different elements have completely random arrangements on the lattice. Short-range order has, however, been reported in a solid-solution NiCoCr alloy subjected to various processing and irradiation conditions [9,11,74]. Together with the present results, this indicates that the assumption of complete randomness is not necessarily valid in irradiated material even at early stages of radiation damage accumulation. Extended X-ray absorption fine structure analysis and scattering measurements reveal that the vibration of Ni-Cr and Ni-Co bonds is one-order of magnitude smaller than that of other pairs, suggesting Cr is favorably bonded with Ni and Co. This local structure is also confirmed by ab initio and MD calculations. Alloy properties are closely related to their structures, although the atomic-level structural impact is unknown. Short-range order calls attention to composition fluctuation at the atomic level and highlights the necessity of fully interpreting all constituents, as the scenario of a totally random arrangement is insufficient. Importantly, the analysis of the electronic structure reveals that the capability for charge transfer between neighboring atoms is affected by the 3*d* electron count [9,30,75]. Compared with the late 3*d* transition elements Ni and Co, the partially filled 3*d* electron states and their densities in Fe and Cr are flexible, readily accommodating defects. This discovery provides insights into unusual properties controlling energy dissipation and defect evolution mechanisms leading towards ultimate suppression of radiation degradation. Further, it clearly demonstrates the importance and suggests a new design strategy of alloying elements with partially filled *d* electron shells to produce beneficially modified energy landscapes for altering mass transport properties.

5. Summary

We show that elemental segregation takes place already at very early stages of radiation damage in single-phase concentrated solid solution alloys (SP-CSAs), well below 1 dpa. This is observed

through the atomic-level segregation of Ni around mono-vacancy-type damage in Ni-based SP-CSAs composed of 3*d* transition metals in the form of binary, ternary and 4-element NiCoFeCr alloys. We arrive at this conclusion by following the evolution of positron annihilation signals as a function of irradiation dose in single crystal samples, complemented by molecular dynamics simulations in the same model systems for high entropy alloys (HEAs). This manifestation of short-range order calls attention to composition fluctuations at the atomic level in HEAs and highlights the necessity of fully interpreting all constituents, as the scenario of a totally random arrangement is clearly insufficient. Our discovery also provides insights into unusual properties controlling energy dissipation and defect evolution mechanisms leading towards ultimate suppression of radiation degradation.

Declaration of Competing Interest

The authors declare that they have no known competing financial interests or personal relationships that could have appeared to influence the work reported in this paper.

Acknowledgments

The work performed by the researchers at Aalto University was supported by the Academy of Finland grants 285809, 293932 and 319178. The work performed by the researchers in USA was supported as part of the Energy Dissipation to Defect Evolution (EDDE), an Energy Frontier Research Center funded by the U.S. Department of Energy, Office of Science, Basic Energy Sciences, under contract number DE-AC05-00OR22725. Ion irradiations were performed at the Ion Beam Materials Laboratory (IBML, https://ibml.utk.edu/) located on the campus of the University of Tennessee, Knoxville. The University of Helsinki part of this work has been carried out within the framework of the EUROfusion Consortium and has received funding from the Euratom research and training programme 2014–2018 under grant agreement No 633053. The views and opinions expressed herein do not necessarily reflect those of the European Commission.

Supplementary materials

Supplementary material associated with this article can be found, in the online version, at doi:10.1016/j.actamat.2020.06.024.

References

[1] Z. Li, K.G. Pradeep, Y. Deng, D. Raabe, C.C. Tasan, Metastable high-entropy dual-phase alloys overcome the strength-ductility trade-off, Nature 534 (2016) 227.
[2] M.H. Tsai, J.W. Yeh, High-Entropy Alloys: A Critical Review, Mater. Res. Lett. 2 (2014) 107.
[3] B. Gludovatz, A. Hohenwarter, D. Catoor, E.H. Chang, E.P. George, R.O. Ritchie, A fracture-resistant high-entropy alloy for cryogenic applications, Science 345 (2014) 1153.
[4] D.B. Miracle, O.N. Senkov, A critical review of high entropy alloys and related concepts, Acta Mater 122 (2017) 448.
[5] H.Y. Diao, R. Feng, K.A. Dahmen, P.K. Liaw, Fundamental deformation behavior in high-entropy alloys: An overview, Curr. Opin. Solid State Mater. Sci. 21 (2017) 252.
[6] Y. Zhang, S. Zhao, W.J. Weber, K. Nordlund, F. Granberg, F. Djurabekova, Atomic-level Heterogeneity and Defect Dynamics in Concentrated Solid-Solution Alloys, Curr. Opin. Solid State Mater. Sci. 21 (2017) 221.
[7] C. Lu, L. Niu, N. Chen, K. Jin, T. Yang, P. Xiu, Y. Zhang, F. Gao, H. Bei, S. Shi, M-R He, I.M. Robertson, W.J. Weber, L. Wang, Enhancing radiation tolerance by controlling defect mobility and migration pathways in multicomponent single-phase alloys, Nat. Commun. 7 (2016) 13564.
[8] Y. Zhang, G.M. Stocks, K. Jin, C. Lu, H. Bei, B.C. Sales, L. Wang, L.K. Beland, R.E. Stoller, G.D. Samolyuk, M. Caro, A. Caro, W.J. Weber, Influence of chemical disorder on energy dissipation and defect evolution in concentrated solid solution alloys, Nat. Commun. 6 (2015) 8736.
[9] Y. Zhang, T. Egami, W.J. Weber, Dissipation of radiation energy in concentrated solid-solution alloys: Unique defect properties and microstructural evolution, MRS Bulletin 44 (2019) 798.
[10] K. Jin, C. Lu, L. Wang, J. Qu, W.J. Weber, Y. Zhang, H. Bei, Effects of compositional complexity on the ion-irradiation induced swelling and hardening in Ni-containing equiatomic alloys, Scr. Mater. 119 (2016) 65.
[11] F.X. Zhang, S. Zhao, K. Jin, H. Xue, G. Velisa, H. Bei, R. Huang, P. Ko, D.C. Pagan, J.C. Neuefeind, W.J. Weber, Y. Zhang, Local Structure and Short-Range Order in a NiCoCr Solid Solution Alloy, Phys. Rev. Lett. 118 (2017) 205501.
[12] Y.Y. Chen, U.T. Hong, H.C. Shih, J.W. Yeh, T. Duval, Electrochemical kinetics of the high entropy alloys in aqueous environments—a comparison with type 304 stainless steel, Corros. Sci. 47 (2005) 2679.
[13] Y. Qiu, S. Thomas, M.A. Gibson, H.L. Fraser, N. Birbilis, Corrosion of high entropy alloys, NPJ Mater. Degrad. 1 (2017) 15.
[14] Y. Shi, B. Yang, P.K. Liaw, Corrosion-resistant high-entropy alloys: a review, Metal 7 (2017) 2.
[15] S.A. Norris, J. Samela, L. Bukonte, M. Backman, F. Djurabekova, K. Nordlund, C.S. Madi, M.P. Brenner, M.J. Aziz, Molecular dynamics of single-particle impacts predicts phase diagrams for large scale pattern formation, Nat. Commun. 2 (2011) 276.
[16] C.-C. Fu, J.D. Torre, Willaime F, Bocquet J.-L, A. Barbu, Multiscale modelling of defect kinetics in irradiated iron, Nat. Mater. 4 (2005) 68.
[17] G.S. Was, Fundamentals of Radiation Materials Science: Metals and Alloys, Springer, 2017.
[18] T.R. Allen, G.S. Was, Modeling radiation-induced segregation in austenitic Fe–Cr–Ni alloys, Acta Mater 46 (1998) 3679.
[19] A.J. Ardell, P. Bellon, Radiation-induced solute segregation in metallic alloys, Curr. Opin. Solid State Mater. Sci. 20 (2016) 115.
[20] I.J. Beyerlein, A. Caro, M.J. Demkowicz, N.A. Mara, A. Misra, B.P. Uberuaga, Radiation damage tolerant nanomaterials, Materials Today 16 (2013) 443.
[21] S. Zhao, G.M. Stocks, Y. Zhang, Defect energetics of concentrated solid-solution alloys from *ab initio* calculations: $Ni_{0.5}Co_{0.5}$, $Ni_{0.5}Fe_{0.5}$, $Ni_{0.8}Fe_{0.2}$ and $Ni_{0.8}Cr_{0.2}$, Phys. Chem. Chem. Phys. 18 (2016) 24043.
[22] M.-R. He, S. Wang, S. Shi, K. Jin, H. Bei, K. Yasuda, Matsumura S, K. Higashida, I.M. Robertson, Mechanisms of radiation-induced segregation in CrFeCoNi-based single-phase concentrated solid solution alloys, Acta Mater 126 (2017) 182.
[23] C. Lu, T. Yang, K. Jin, N. Gao, P. Xiu, Y. Zhang, F. Gao, H. Bei, Y. Dong, L. Wang, Radiation-induced segregation on defect clusters in single-phase concentrated solid-solution alloys, Acta Mater 127 (2017) 98.
[24] K. Nordlund, S.J. Zinkle, A.E. Sand, F. Granberg, R.S. Averback, R. Stoller, T. Suzudo, L. Malerba, F. Banhart, W.J. Weber, F. Willaime, S. Dudarev, D. Simeone, Primary radiation damage: A review of current understanding and models, J. Nucl. Mater. 512 (2018) 450.
[25] L. Koch, F. Granberg, T. Brink, K. Albe, F. Djurabekova, K. Nordlund, Local segregation versus irradiation effects in high-entropy alloys: Steady-state conditions in a driven system, J. Appl. Phys 122 (2017) 105106.
[26] A. Barashev, Y.N. Osetsky, H. Bei, C. Lu, L. Wang, Y. Zhang, Chemically-biased diffusion and segregation impedes void growth in irradiated Ni-Fe alloys, Curr. Opin. Solid State Mater. Sci. 23 (2019) 92.
[27] S. Zhao, Y. Osetsky, Y. Zhang, Preferable diffusion in concentrated solid solution alloys: NiFe, NiCo and NiCoCr, Acta Mater 128 (2017) 391.
[28] S. Shi, H. Bei, I.M. Robertson, Impact of alloy composition on one-dimensional glide of small dislocation loops in concentrated solid solution alloys, Mater. Sci. Eng. A. 700 (2017) 617.
[29] G. Velisa, E. Wendler, S. Zhao, K. Jin, H. Bei, W.J. Weber, Y. Zhang, Delayed damage accumulation by athermal suppression of defect production in concentrated solid solution alloys, Mater. Res. Lett. 6 (2018) 136.
[30] Y. Zhang, X. Wang, Y. Osetsky, Y. Tong, R. Harrison, S.E. Donnelly, D. Chen, Y. Wang, H. Bei, B.C. Sales, K.L. More, P. Xiu, L. Wang, W.J. Weber, Effects of 3d electron configurations on helium bubble formation and void swelling in concentrated solid-solution alloys, Acta Mater. 181 (2019) 519.
[31] F. Tuomisto, I. Makkonen, Defect identification in semiconductors with positron annihilation: Experiment and theory, Rev. Mod. Phys. 85 (2013) 1583.
[32] A. van Veen, H. Schut, J. de Vries, R.A. Hakvoort, M.R. Ijpma, Analysis of positron profiling data by means of "VEPFIT", AIP Conf. Proc. 218 (1991) 171.
[33] I. Makkonen, M. Hakala, M.J. Puska, Modeling the momentum distributions of annihilating electron-positron pairs in solids, Phys. Rev. B 73 (2006) 035103.
[34] I. Makkonen, M. Hakala, M. J. Puska, Calculation of valence electron momentum densities using the projector augmented-wave method, J. Phys. Chem. Solids 66 (2005) 1128.
[35] P.E. Blöchl, Projector augmented-wave method, Phys. Rev. B 50 (1994) 17953.
[36] G. Kresse, J. Furthmüller, Efficient iterative schemes for ab initio total-energy calculations using a plane-wave basis set, Phys. Rev. B 54 (1996) 11169.
[37] G. Kresse, J. Furthmüller, Efficiency of ab-initio total energy calculations for metals and semiconductors using a plane-wave basis set, Comput. Mater. Sci. 6 (1996) 15.
[38] G. Kresse, D. Joubert, From ultrasoft pseudopotentials to the projector augmented-wave method, Phys. Rev. B 59 (1999) 1758.
[39] E. Boronski, R.M. Nieminen, Electron-positron density-functional theory, Phys. Rev. B 34 (1986) 3820.
[40] M. Alatalo, B. Barbiellini, M. Hakala, H. Kauppinen, T. Korhonen, M.J. Puska, K. Saarinen, P. Hautojärvi, R.M. Nieminen, Theoretical and experimental study of positron annihilation with core electrons in solids, Phys. Rev. B 54 (1996) 2397.
[41] Y. Zhang, M.L. Crespillo, H. Xue, K. Jin, C.-H. Chen, C.L. Fontana, J.T. Graham, W.J. Weber, New ion beam materials laboratory for materials modification and irradiation effects research, Nucl. Instrum. & Meth. B 338 (2014) 19.

[42] N. Sellami, A. Debelle, M.W. Ullah, H.M. Christen, J.K. Keum, H. Bei, H. Xue, W.J. Weber, Y. Zhang, Effect of electronic energy dissipation on strain relaxation in irradiated concentrated solid solution alloys, Curr. Opin. Solid State Mater. Sci. 23 (2019) 107.
[43] S. Mu, R.J. Olsen, B. Dutta, L. Lindsay, G.D. Samolyuk, T. Berlijn, E.D. Specht, K. Jin, H. Bei, T. Hickel, B.C. Larson, G- M. Stocks, Unfolding the complexity of phonon quasi-particle physics in disordered materials, NPJ Comput. Mater. 6 (2020) 4.
[44] Z. Wu, H. Bei, Microstructures and mechanical properties of compositionally complex Co-free FeNiMnCr18 FCC solid solution alloy, Mater. Sci. Eng. A 640 (2015) 217.
[45] L.K. Béland, Yu.N. Osetsky, R.E. Stoller, Atomistic material behavior at extreme pressures, NPJ Comput. Mater. 2 (2016) 16007.
[46] J.F. Ziegler, J.P. Biersack, M.D. Ziegler, SRIM–The Stopping and Range of Ions in Solids, SRIM Co., Chester, MD, 2008.
[47] W.J. Weber, Y. Zhang, Predicting damage production in monoatomic and multi--elemental targets using stopping and range of ions in matter code: Challenges and recommendations, Curr. Opin. Solid State Mater. Sci. 23 (2019) 100757.
[48] Z. Wu, Temperature and alloying effects on the mechanical properties of equiatomic FCC solid solution alloys, Ph. D Dissertation in Materials Science and Engineering, Knoxville, 2014.
[49] F. Granberg, K. Nordlund, M.W. Ullah, K. Jin, C. Lu, H. Bei, L.M. Wang, F. Djurabekova, W.J. Weber, Y. Zhang, Mechanism of radiation damage reduction in equiatomic multicomponent single phase alloys, Phys. Rev. Lett. 116 (2016) 135504.
[50] E. Levo, F. Granberg, C. Fridlund, K. Nordlund, F. Djurabekova, Radiation damage buildup and dislocation evolution in Ni and equiatomic multicomponent Ni-based alloys, J. Nuclear Mater. 490 (2017) 323.
[51] K. Nordlund, M. Ghaly, R.S. Averback, M. Caturla, T. Diaz de la Rubia, J. Tarus, Defect production in collision cascades in elemental semiconductors and fcc metals, Phys. Rev. B 57 (1998) 7556.
[52] S. Zhang, K. Nordlund, F. Djurabekova, F. Granberg, Y. Zhang, T.S. Wang, Radiation damage buildup by athermal defect reactions in nickel and concentrated nickel alloys, Mater. Res. Lett. 5 (2017) 433.
[53] J. Moreno-Martin, U. Conrad, H. Urbassek, A. Gras-Marti, Fractal structure of collision cascades, Nucl. Instr. and Meth. B 48 (1990) 404.
[54] A. Vehanen, P. Hautojärvi, J. Johansson, J. Yli-Kauppila, P. Moser, Vacancies and carbon impurities in α-iron: Electron irradiation, Phys. Rev. B 25 (1982) 762.
[55] A. G. Balogh, L. Bottyan, G. Brauer, I. Dezsi, B. Molnar, Positron lifetime and Doppler studies of Co-Si alloys, J. Phys. F: Metal Phys. 16 (1986) 1725.
[56] J. Cizek, I. Prochazka, M. Cieslar, I. Stulikova, F. Chmelik, R. K. Islamgaiev, Positron-Lifetime Investigation of Thermal Stability of Ultra-Fine Grained Nickel, Phys. Status Solidi (a) 191 (2002) 391.
[57] T. Troev, A. Markovski, S. Peneva, T. Yoshiie, Positron lifetime calculations of defects in chromium containing hydrogen or helium, J. Nucl. Mater. 359 (2006) 93.
[58] M. Elsayed, R. Krause-Rehberg, C. Eisenschmidt, N. Eissmann, B. Kieback, Defect Study in CoCrFeMnNi high entropy alloy by positron annihilation lifetime spectroscopy, Phys. Status Solidi 215 (2018) 1800036.
[59] A. Somoza, M.P. Petkov, K.G. Lynn, A. Dupasquier, Stability of vacancies during solute clustering in Al-Cu-based alloys, Phys. Rev. B 65 (2002) 094107.
[60] S. Abhaya, R. Rajaraman, R.M. Sarguna, P.K. Parida, C. David, G. Amarendra, Defect microstructure in high temperature Ni^+ implanted FeCrCoNi-a positron beam study, J. Alloys Comp 806 (2019) 780.
[61] A.P. Druzhkov, S.E. Danilov, D.A. Perminov, V.L. Arbuzov, Effect of phosphorus on vacancy-type defect behaviour in electron-irradiated Ni studied by positron annihilation, J. Nuclear Mater. 457 (2015) 48.
[62] P. Folegati, I. Makkonen, R. Ferragut, M.J. Puska, Analysis of electron-positron momentum spectra of metallic alloys as supported by first-principles calculations, Phys. Rev. B 75 (2007) 054201.
[63] R.S. Brusa, W. Deng, G.P. Karwasz, A. Zecca, Doppler-broadening measurements of positron annhilation with high-momentum electrons in pure elements, Nucl. Instr. Methods B 194 (2002) 159.
[64] P. Hautojärvi and C. Corbel, Positron Spectroscopy of Defects in Metals and Semiconductors, Proceedings of the International School of Physics Enrico Fermi Course CXXV, Eds. A. Dupasquier and A. P. Mills, Jr. (IOS Press, Amsterdam), p. 491.
[65] O.E. Boev, M.J. Puska, R.M. Nieminen, Electron and positron energy levels in solids, Phys. Rev. B 36 (1987) 7786.
[66] J. Heikinheimo, K. Mizohata, J. Räisänen, T. Ahlgren, P. Jalkanen, A. Lahtinen, N. Catarino, E. Alves, F. Tuomisto, Direct observation of mono-vacancy and self--interstitial recovery in tungsten, APL Mater 7 (2019) 021103.
[67] M. Vaidya, S. Trubel, B.S. Murty, G. Wilde, S.V. Divinski, Ni tracer diffusion in CoCrFeNi and CoCrFeMnNi high entropy alloys, J. Alloys Comp. 688 (2016) 994.
[68] M. Vaidya, K. G. Pradeep, B. S. Murty, G. Wilde, S. V. Divinski, Radioactive isotopes reveal a non sluggish kinetics of grain boundary diffusion in high entropy alloys, Sci. Rep. 7 (2017) 12293.
[69] M. Vaidya, K. G. Pradeep, B. S. Murty, G. Wilde, S. V. Divisnki, Bulk tracer diffusion in CoCrFeNi and CoCrFeMnNi high entropy alloys, Acta Mater. 146 (2018) 211.
[70] T. Iwata, A. Iwase, Damage Production and Annealing in Ion-Irradiated Fcc Metals, Radiat. Effects Defects Solids 113 (1990) 135.
[71] J. Zinkle, Radiation-Induced Effects on Microstructure, in: R. Kronings (Ed.), Comprehensive Nuclear Materials, Elsevier, 2012, p. 65.
[72] Y.N. Osetskiy, L. Beland, A. Barashev, Y. Zhang, On the existence and origin of sluggish diffusion in chemically disordered concentrated alloys, Curr. Opin. Solid State Mater. Sci. 22 (2018) 65.
[73] E. Lu, I. Makkonen, K. Mizohata, Z. Li, J. Räisänen, F. Tuomisto, Effect of interstitial carbon on the evolution of early-stage irradiation damage in equi-atomic FeMnNiCoCr high-entropy alloys, J. Appl. Phys. 127 (2020) 025103.
[74] Q.-J. Li, H. Sheng, E. Ma, Strengthening in multi-principal element alloys with local-chemical-order roughened dislocation pathways, Nat. Commun. 10 (2019) 3563.
[75] S. Zhao, T. Egami, M. Stocks, Y. Zhang, Effect of d electrons ondefect properties in equiatomic NiCoCr and NiCoFeCr concentrated solid solution alloys, Phys. Rev. Mater. 2 (2018) 013602.